Development of Mn-based novel magnetic materials through lattice engineering

T. Shima[1], M. Doi[1], H. Okada[1], M. Tsujikawa[2,3], M. Shirai[2,3]

[1] Faculty of Engineering, Tohoku Gakuin University, Tagajo 985-8537, Japan

[2] Research Institute of Electrical Communication, Tohoku University, Sendai 980-8577, Japan

[3] Center for Spintronics Research Network, Tohoku University, Sendai 980-8577, Japan

High performance rare earth based permanent magnets have been used widely as a magnetomotive force in applications such as motors, actuators and sensors for $Nd_2Fe_{14}B$ alloy's large magnetocrystalline anisotropy (K_{u1} = 4.5 x 10^6 J/m^3 at room temperature) and relatively high magnetization (M_s = 1.6T). Recently, the consumption of Nd-Fe-B sintered magnets has increased due to the utilization for hybrid, plug-in hybrid and electric vehicles (HV's, PHEV's and EV's). However, due to the scarce natural resource of key elements such as Dy and Tb, a lot of efforts have been done to find another permanent magnet materials instead of rare earth based alloys. One of the candidate materials is Mn-based alloys. The binary Heusler-like compounds Mn_xGa (x = 2~3) have attracted much attention due to its high Curie temperature and large magnetic anisotropy[1,2]. However, as shown in Fig. 1, for Mn compositions of x =2~3, the tetragonal $D0_{22}$ structure possesses ferrimagnetic property, and consequently it demonstrates a low saturation magnetization. Recent studies revealed that Mn_xGa alloy with the $D0_{22}$ structure demonstrated large coercivities[3,4] in exceeding 2 T at room temperature, this arise from a large magnetocrystalline anisotropy (K ~ 10 Merg/cm^3). Such high magnetocrystalline anisotropy makes Mn_xGa alloy possible alternative to rare earth and noble metal based magnets in future permanent magnet applications. In this talk, in addition to the theoretical prediction, our recent activities of the lattice engineering on the preparation and evaluation of the bulk and film samples[5,6] for $D0_{22}$ and $L1_0$ structure of $Mn_x(Ga, Ge)$ alloys with the addition of third elements will be introduced.

Mn-based bulk alloys have been prepared by arc melting in an argon gas atmosphere. All samples were re-melted at eight times to perform homogenization. The samples were powdered by diamond file or grinding in an agate. Then, the powders have been vacuum sealing in a quartz tube and annealed from 350℃ to 550℃ at Muffle furnace. For the preparation of film samples, MgO(100) single crystal substrates were selected and they were prepared using an ultra-high vacuum (UHV) electron beam evaporation system or UHV sputtering system. The substrate was heated to T_s = 300 ℃ during the deposition and they were annealed at 300 ~ 500 ℃. The crystal and surface structures were investigated by XRD and AFM. Composition of samples was analyzed by EDX. Magnetic properties were measured by using a SQUID or PPMS-VSM, and M_s and K_u for each thin film were evaluated from magnetization curves.

Reference
1) H. Niida, T. Hori, H. Onodera, Y. Yamaguchi, and Y. Nakagawa, J. Appl. Phys. **79**, 5946 (1996).
2) J. Winterlik, B. Balke, G. H. Fecher, and C. Felser, M. C. M. Alves, F. Bernardi, and J. Morais, Phys. Rev. B **77**, 054406 (2008).
3) F. Wu, S. Mizukami, D. Watanabe, H. Naganuma, M. Oogane, Y. Ando, and T. Miyazaki, Appl. Phys. Lett. **94**, 122503 (2009).
4) H. Kurt, K. Rode, M. Venkatesan, P. Stamenov, and J. M. D. Coey, Phys. Rev. B **83**, 020405 (2011).
5) Y. Takahashi, H. Makuta, T. Shima and M. Doi, T. Magn. Soc. Japan, **1**, 30-33 (2017).
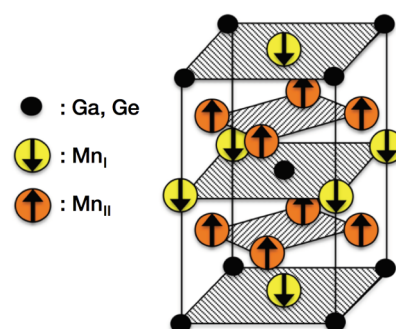6) H. Makuta, Y. Takahashi, T. Shima and M. Doi, T. Magn. Soc. Japan, **1**, 26-29 (2017).

Fig. 1 Crystal structure of DO_{22}-type $Mn_3(Ga, Ge)$ ordered alloy (magnetic structure).

Strain-induced magnetic anisotropy in spinel ferrites

Hideto Yanagihara[1]
[1]Institute for Applied Physics, Univ. of Tsukuba, Tsukuba, 805-8573, Japan

Magnetic anisotropy is one of the more important properties of magnetic materials. Since the magnetic anisotropy arises from spin-orbit interaction accompanying local/global symmetry reduction, both the anisotropy energy and sign can be controlled by a relatively slight perturbation such as lattice strain. Because of their large spin-orbit interaction, most magnetic materials exhibiting large magnetic anisotropy energy contain heavy metals or rare earth elements such as palladium, platinum, bismuth, neodymium samarium and so on.

Among some $3d$-transition metal oxides with degeneracy arising from their peculiar electron configuration in the t_{2g} states, orbital momentum of ~1 μ_B is seen on the $3d$ ions. If the relatively large orbital momentum couples with the spin momentum, a large magnetic anisotropy can emerge even in the absence of rare metals. In fact, some spinel ferrites containing Co^{2+} ions have been known to show large anisotropy as well as high coercivity[1]. The crystal field for Co^{2+} ions in a bulk cobalt ferrite is primarily cubic because of the Co^{2+} ions being located at the octahedral sites (B-sites). Moreover, since the B-site cations of the second nearest neighbor form a trigonal crystal field, the t_{2g} electron configuration of the Co^{2+} ions is split into a single lowest level and two degenerate levels. Since the single electron occupying the doubly degenerate states has ~1 μ_B, it therefore exhibits a large cubic magnetic anisotropy K_1 as well as magnetization enhancement[2,3].

When cobalt ferrite is grown as epitaxially strained thin films, the films undergo compressive/tensile stress depending on the lattice misfit between the cobalt ferrite and the substrate. The induced uniaxial magnetic anisotropy K_u from the uniaxial strain (or tetragonal distortion) can be understood by a phenomenological treatment within the framework of the magnetoelastic effect. The induced K_u is also interpreted by an electronic model as equivalent to K_1 of the bulk cobalt ferrite[4]. Since the tetragonal distortion also splits the t_{2g} electron configuration of Co^{2+} into a single lowest level and double degenerate levels like in the bulk case, a significantly large K_u is induced. The epitaxial films of cobalt ferrite grown on a square lattice such as the surface of $MgO(001)$(tensile stress) and $MgAl_2O_4(001)$(compressive stress) are tetragonally distorted and consequently show K_u. If the induced K_u is greater than the demagnetization energy of $2\pi M_s^2 \sim$ 1.0 $Merg/cm^3$, the film exhibits perpendicular magnetization. Practically, we have demonstrated that a high-quality epitaxial film of $Co_{0.75}Fe_{2.25}O_4(001)$ /$MgO(001)$ exhibits K_u as large as 10.0 $Merg/cm^3$.[5]

Thus, in order to develop new candidate materials for permanent magnets, it seems to be a promising strategy to intentionally induce a lattice strain in spinel ferrites containing Co^{2+} ions. According to the phenomenological model, a larger distortion produces a higher magnetic anisotropy in a linear relationship. However, this picture is valid only for a small distortion. To evaluate the potential of cobalt ferrite as a large magnetic anisotropy material, it is worth investigating how we can apply epitaxial strain and induce a large K_u. Moreover, by introducing a large lattice distortion into the bulk or particles of cobalt-based spinel ferrite, this magnetic compound may become a new candidate material of the rare-earth free magnet. In this presentation, we will show our attempts to enhance the magnetic anisotropy of cobalt ferrite in both film- and particle-forms.

Epitaxial films of $Co_{0.75}Fe_{2.25}O_4(001)$ were grown by reactive magnetron sputtering with an alloy target. In order to induce a large lattice distortion into the films, we investigated many different oxide substrates and buffer layers. We found that the inverse spinel of $Mg_2SnO_4(001)$ is appropriate as a buffer layer with a large lattice misfit and that a 10-nm-thick $Co_{0.75}Fe_{2.25}O_4(001)$ film grown on $Mg_2SnO_4(001)$ exhibits K_u larger than 25.0 $Merg/cm^3$. To our knowledge, this is the largest K_u ever reported in a spinel ferrite thin film. Although the lattice misfit is as large as ~3.1%, the induced K_u can be quantitatively explained by the magnetoelastic theory.

Since lattice strain of several percent effectively induces large K_u in cobalt ferrite, we attempted to spontaneously distort the spinel ferrite particles via the Jahn-Teller effect. Jahn-Teller ions such as Cu^{2+} were chosen on a trial basis though expected saturation magnetization for this compound is small. $(Cu, Co)Fe_2O_4$ particles were prepared by coprecipitation method followed by flux treatment of KBr. After the flux treatment, $(Cu, Co)Fe_2O_4$ with a cubic spinel was obtained. Post annealing process in the atmosphere facilitated the crystal structure transformation from cubic to tetragonal. Although the magnetization curve of $Co_{0.1}Cu_{0.9}Fe_2O_4$ particles grown before the post annealing process shows coercivity as small as

300 Oe, after annealing 2200 Oe of coercivity was observed, reflecting the induced tetragonal distortion. All the experimental results indicate that Jahn-Teller ions definitely induce local/global distortion into the spinel structure and the distortion increases the magnetic anisotropy through the locally distorted crystal field of the Co^{2+} ions.

References
[1] S. Chikazumi, *Physics of Ferromagnetism* (Wiley, 1964).
[2] J.C. Slonczewski, Phys. Rev. **110**, 1341 (1958).
[3] J.C. Slonczewski, J. Appl. Phys. **32**, S253 (1961).
[4] J. Inoue, T. Niizeki, H. Yanagihara, H. Itoh, and E. Kita, AIP Adv. **4**, 27111 (2014).
[5] T. Niizeki, Y. Utsumi, R. Aoyama, H. Yanagihara, J. Inoue, Y. Yamasaki, H. Nakao, K. Koike, and E. Kita, Appl. Phys. Lett. **103**, 162407 (2013).

Recent progress and future development of synchrotron X-ray analysis

of high-performance permanent magnets

T. Nakamura[*], Y. Matsuura[**], R. Tamura[***], K. Sumitani, K. Kajiwara, K. Toyoki, D. Billington, H. Okazaki, Y. Kotani, and S. Hirosawa[*]

(JASRI, [*]ESICMM/NIMS, [**]RIAS, [***] Tokyo Univ. of Sci.)

Studies of the magnetization reversal process provide a key clue in uncovering the coercivity mechanism of permanent magnets. The magnetic domain structure inside a magnet forms a three-dimensional network in which one magnetic domain couples with its neighboring ones which have opposite directions of magnetization and are separated by inter- and intra-grain magnetic domain walls. When the magnetization is saturated by an external magnetic field that is sufficiently larger than the magnetic anisotropy field, the magnetic domain structure vanishes. Therefore, a clear-cut aim of studying the magnetization reversal process is to understand how the reversed magnetic domains are initially nucleated as the external magnetic field decreases and how the magnetic domain structure changes with other nucleation events and/or magnetic-domain-wall displacements.

Since their invention in 1984 [1], Nd-Fe-B magnets have been the best permanent magnets and have become an indispensable material for various electric products, hybrid vehicles, and power generators, which are now key technologies for energy sustainability. In the case of Nd-Fe-B sintered magnets, it is known that the coercivity in a polished surface is rather moderate in comparison to that of the bulk [2]. In stark contrast to the significantly decreased coercivity of the polished surface, we presented that the coercivity of the fractured surface closely resembles that of the bulk in a previous study [3]. The higher coercivity of the fractured surface is attributed to the particular way in which Nd-Fe-B sintered magnets fracture, where the majority of the fractured surface remains covered with a thin layer of the grain boundary phase. Although the similarity between the fractured surface and bulk coercivities cry out for magnetic domain observations of the fractured surface, conventional magnetic domain observations using Kerr microscopy, magnetic force microscopy, and photoelectron emission microscopy, have only been conducted on polished surfaces or thin films.

In order to observe the magnetic domain structure in the fractured surface under various magnetic fields, we developed a scanning soft X-ray spectromicroscope equipped with a superconducting magnet with a maximum magnetic field of ±8 T. When used in combination with X-ray photons of opposite helicity, and total-electron-yield detection, magnetic domain observations of the fractured surface become possible. Fig.1 shows the magnetic domain structure of the fractured surface of a Dy-free Nd-Fe-B sintered magnet (with composition $Nd_{14.0}Fe_{79.7}Cu_{0.1}B_{6.2}$) at an applied magnetic field of -0.7 T (after almost saturating the magnet at +3.0 T). In the figure, both the microstructure and the magnetic domain contrast are clearly observed. The magnetic field dependence of the magnetic domains has shown that the precise location in which reversed domains
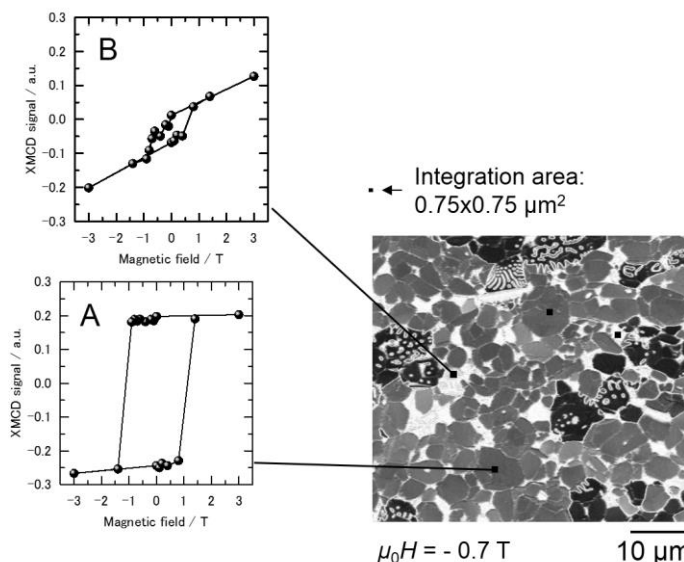

Fig.1 Magnetic domain structure of a Nd-Fe-B sintered magnet under an applied magnetic field of -0.7 T (*right*). Magnetic field dependence of XMCD intensity, A and B, give the local magnetic hysteresis loops in the selected grains.

are initially generated is always identical, and independent of whether the magnetic field is increased or decreased. Further analysis has allowed us to characterize the local magnetic hysteresis (MH) loops for areas ~ 100 nm^2. The observed local MH loops show a wide variety of magnetization reversal characteristics depending on the particular grain. As an example, we have plotted the MH loops for two different grains in Fig.1, labeled A and B, whose magnetization reversal characteristics are rather different. The observed differences between grains suggest that the magnetization reversal of each grain is very sensitive to the local effective magnetic field.

To understand the variety of local MH curves observed, we need to understand the local effective magnetic field. Prohibitively, the local effective magnetic field is very difficult to determine because it depends upon the stray magnetic field from the surrounding magnetic grains, which in-turn depends on the precise orientation of each grain, together with their intrinsic coercivity and the exchange coupling with the grains in the sub-surface layers.

Unfortunately, the angle of the easy magnetic (*c*-)axis between each $Nd_2Fe_{14}B$ grain and the intended direction cannot be estimated from the local MH curves. Generally, the electron back-scatter diffraction (EBSD) technique is the most popular method to analyze the grain orientation. However, EBSD cannot be applied to the irregular fractured surface of our sample (which is the favorable target for magnetic domain observations). Therefore, we are developing a scanning X-ray micro-diffraction (SXMD) instrument which can probe any surface, independent of their roughness and irregularity. Moreover, the SXMD has a much longer probing depth than that of EBSD meaning that it is not necessary to worry about the surface state of the target sample, which makes sample preparation much easier. Fig. 2 shows a 3D schematic diagram of the SXMD apparatus under development at SPring-8.
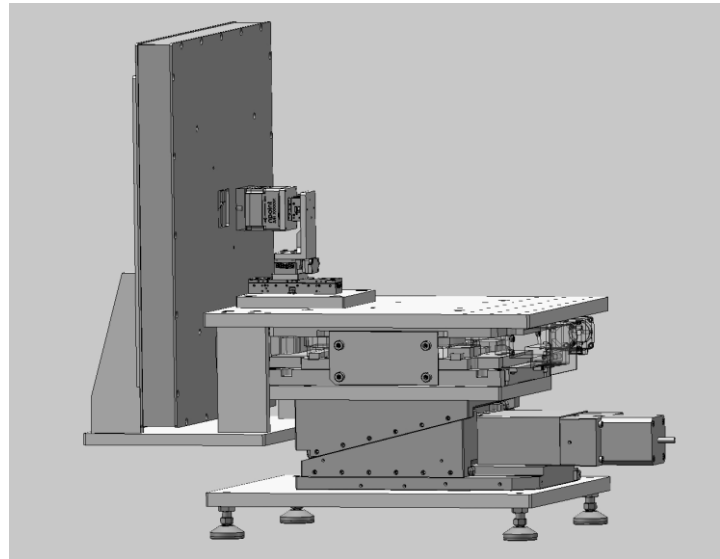

Fig.2 3D schematic diagram of the scanning X-ray micro-diffraction apparatus under development at SPring-8.

In this presentation, I will discuss our research involving the use of synchrotron X-ray diffraction to investigate the crystalline phases that constitute the microstructure, and scanning soft X-ray spectromicroscopy techniques to directly observe magnetization reversal process in Nd-Fe-B sintered magnets. I will also describe the progress made in the development of the scanning X-ray micro-diffraction instrument.

Acknowledgements

References

[1] M. Sagawa, S. Fujimura, N. Togawa, H. Hashimoto, and Y. Matsuura, J. Appl. Phys. **55**, 2083 (1984).
[2] K. Kobayashi, M. Nakamura, and K. Urushibata, J. Appl. Phys. **117**, 173909 (2015).
[3] T. Nakamura, A. Yasui, Y. Kotani, T. Fukagawa, T. Nishiuchi, H. Iwai, T. Akiya, T. Ohkubo, Y. Gohda, K. Hono, and S. Hirosawa, Appl. Phys. Lett. **105**, 202404 (2014).

High-throughput experiment of X-ray magnetic circular dichroism spectroscopy with machine learning

T. Ueno[1], H. Hino[2], A. Hashimoto[3], Y. Takeichi[3], and K. Ono[3]

[1]National Institutes for Quantum and Radiological Science and Technology, Sayo 679-5148, Japan
[2]University of Tsukuba, Tsukuba 305-8571, Japan
[3]High Energy Accelerator Research Organization, Tsukuba 305-0801, Japan

X-ray magnetic circular dichroism (XMCD) spectroscopy is a powerful experimental technique to directly probe electronic states and magnetic moments of magnetic materials. Recently, by combining XMCD with X-ray microscopy, it has been able to visualize magnetic domains and conduct spectroscopy experiment in several ten nanometers scale [1]. This method is useful because a specimen with the size of only several square micrometers can be measured. Therefore, one does not need to prepare large single crystal samples. The method is also useful for heterogeneous systems such as microstructures in permanent magnet materials. However, one must scan large area (several 10 μm^2) with fine steps for an application to heterogeneous systems. In the present experimental system [2], typical measurement time is about 2 hours for an area of ~10 μm^2 with 200 energy points. To reduce the measurement time, we examined reduction of the total measurement energy points with a machine learning approach. Gaussian process (GP) modeling [3] was applied to predict an XMCD spectrum from an experimental spectrum with limited energy points.

XMCD spectroscopy experiment was performed at the BL-13A of the Photon Factory, KEK, Japan. Sm $M_{4,5}$ X-ray absorption spectrum (XAS) and XMCD spectrum were measured for an $SmCo_5$ specimen. X-ray energy was scanned around the Sm $M_{4,5}$ edges with a total energy points of 216. GP modeling was performed to predict XAS and XMCD spectra by following way. First, initial 30 data points are sampled with equal separation along the energy axis. GP modeling predicts a spectrum with input of experimental data points. Next sampling point is determined by several methods. After the sampling, a spectrum is predicted again. Orbital and spin magnetic moments, and their ratio were evaluated for each prediction by using magneto-optical sum rules. Measurement is stopped with the convergence of magnetic moments.

We tried three methods to determine next sampling point; (1) energy point with maximum variance of the predicted spectrum, (2) random sampling, and (3) random sampling weighted by maximum variance. Orbital magnetic moment evaluated from predicted spectra converges to reference value in total data points of about 40 points by sampling with maximum variance. Other sampling methods need more data points to converge to reference value. Maximum variance sampling was revealed to be better than other sampling methods in GP modeling of XAS and XMCD spectra. Therefore, total measurement data points are reduced to 1/5 by GP modeling as compared to conventional method [4].

In conclusion, we demonstrated the reduction of the total measurement energy points of XMCD spectra with a machine learning approach. This method enhances efficiency of XMCD spectroscopy experiment.

Reference
[1]   T. Ueno, A. Hashimoto, Y. Takeichi, and K. Ono, AIP Advances **7**, 056804 (2017).
[2]   Y. Takeichi *et al.*, Rev. Sci. Instrum., **87**, 013704 (2016).
[3]   C. E. Rasmussen and C. K. I. Williams, Gaussian Processes for Machine Learning, MIT Press (2006).
[4]   T. Ueno, H. Hino, A. Hashimoto, Y. Takeichi, and K. Ono, INTERMAG2017, GE-07, Dublin, Ireland (2017).

中性子小角散乱によるサイズ分解FORC測定

斉藤耕太郎，上野哲朗*，伊東正朗**，矢野正雄**，庄司哲也**，Zhendong Fu***，Vitaliy
Pipich***，小野寛太
（高エネ研，*物材機構，**トヨタ自動車，***ユーリッヒ中性子科学センター）

Size-resolved FORC measurements using Small Angle Neutron Scattering
K. Saito, T. Ueno*, M. Ito**, M. Yano**, T. Shoji**, Z. Fu***, V. Pipich***, K. Ono
(KEK, *NIMS, **TOYOTA Motor Corp., ***JCNS)

はじめに

　FORC測定はメインループのM_s, M_r, H_c, 角型にしか関心を持っていなかった永久磁石研究に新たな視点をもたらす可能性を持つが、まだ永久磁石材料のFORC図の解釈は発展途上である。磁化反転には反転核形成、磁壁移動、単一粒子反転などスケールの異なる現象が含まれ、これらの作用は全て磁化変化を伴うため理論的にはFORCでも観測できるはずである。しかし、磁化曲線に還元された複数の現象を復元するのは本質的に困難である。中性子小角散乱はバルク試料内部でのスケールの異なる磁気的現象を調べることのできるユニークな実験手法である。磁化測定によるFORCと同様の磁場変化シーケンスでSANSを測定すれば、サイズ分解されたFORCデータに相当する結果が得られる。これらと磁化曲線に基づくFORC測定と合わせた解釈により磁化反転過程をより明確に理解できると考えられる。

実験方法

　はDyフリーNdFeB焼結について様々な磁場において大量のSANSを測定し、サイズ分解されたマルチスケールなFORCに相当するデータを得た。測定時間を短縮するためにFORC図に大きな変化がでる磁場領域に限定した。磁場は試料の容易軸方向に印加した。実験はユーリッヒ中性子科学センターの所有するKWS-3にて行った。

実験結果

　Fig. 1に全測定結果を示す。得られたデータは五つの次元を持つ。FORC測定に必要な二つの磁場パラメータH_r, HとSANSデータが持つ強度Iと散乱ベクトルの向きφと大きさQである。検出器全体のSANS強度をこのH_r-H空間でプロットしたのがFig. 2である。保磁力H_c相当の磁場を含む、磁化が0になる磁場でSANS強度が強いことがわかる。散乱ベクトルの方向と大きさ別に同様のSANS強度マップを作ると、反転磁区の大きさによって反転の起こる磁場が異なることがはっきりと見え、通常の磁化によるFORC測定で求める二階微分量ρを同様に計算するとその差異が明瞭に現れた。このような磁化反転過程における試料内部のスケール別の磁化反転の情報は他の手法では得られない。このことからFORC-like SANSは保磁力機構の解明に貢献すると期待できる。
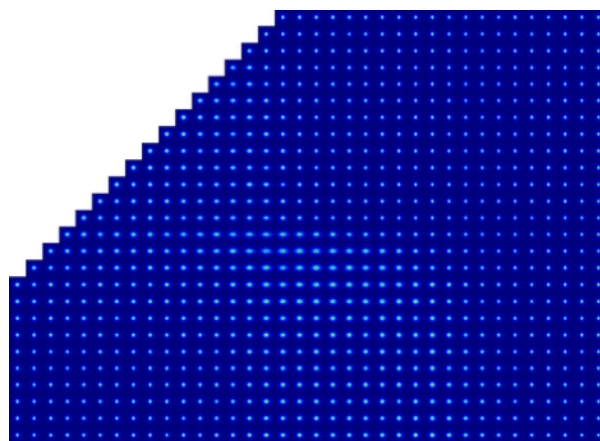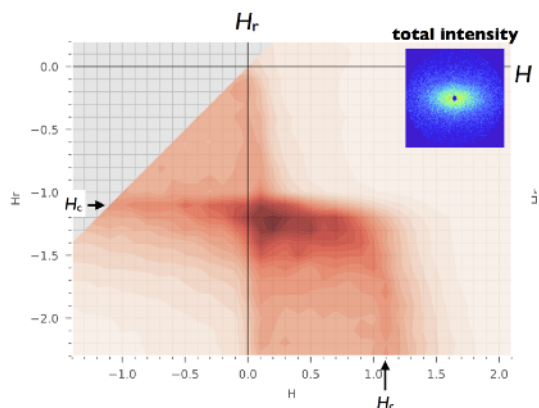

Fig. 1 FORC測定と同様の磁場変化シーケンスによって得られたSANSデータ。軸はFig.2参照。

Fig. 2 H_r-H空間における検出器全体のSANS強度の等高線図。赤の濃い方がカウント数が大きい。

Development of alternating magnetic force microscopy:
Local magnetic domain analysis by advanced magnetic field imaging
with high functionalities for high performance magnets

H. Saito[1], Y. Z. Cao[2], Y. Zhao[2], Y. Suzuki[1], S. Yoshimura[1]

[1] Graduate School of Engineering Science, Akita University, Akita 010-8502

[2] Center for Regional Revitalization in Research and Education, Akita University, Akita 010-8502

For further development of high performance magnets, magnetic domain observation is important to study the relationship between the nanostructure and hard magnetic properties. To observe the magnetic domain structure of magnets, technique with a wide range of imaging area from nm scale to μm scale is required for domain boundary and inside parts magnetic grains. Recently, the magnetic domain observation of NdFeB sintered magnets by X-ray magnetic circular dichroism microscopy revealed that the coercivity of magnetic grains on the grain boundary fractured surface was higher than that on a polished surface and was similar to that of the bulk magnet [1]. Therefore, magnetic domain observation of rough fractured surface is highly desired.

Magnetic force microscopy (MFM) is a technique widely used to investigate the fine magnetic domain structure with relatively high spatial resolution. In order to improve the spatial resolution of MFM, decreasing tip-sample distance is quite important. However, conventional MFM has a difficulty to reduce the tip-sample distance because of topography artifacts near sample surface where short-range forces, such as van der Waals force are dominant. To solve the problem, we have developed alternating magnetic force microscopy (A-MFM). This enables near-surface imaging of DC and AC magnetic fields with high spatial resolution of less than 5 nm by using our developed sensitive ferromagnetic tips [2-3]. Here the definition of spatial resolution is the half of the minimum wavelength where MFM magnetic signal reaches white noise level for the A-MFM image. A-MFM utilizes frequency modulation of a cantilever oscillation generated by an off-resonance alternating magnetic force between a magnetic tip and a magnetic sample.

Table 1 shows the characteristics of conventional MFM and A-MFM. The A-MFM has more functionalities than conventional MFM. For detecting DC magnetic field, A-MFM uses AC magnetic field to drive the tip with periodically changing magnetic moment $M_z^{ac}\cos(\omega_m t)$. For high performance magnets, it is noteworthy that the tip should not be magnetically saturated by magnetic field from the sample. Therefore,

Table 1. Characteristics of conventional MFM and Alternating MFM.

| Characteristic features	Conventional MFM	Alternating MFM
Magnetic field measurement near sample surface	×	○ [All magnetic tips]
Separated detection of magnetic field	× (including short range forces)	○ [All magnetic tips]
Polarity & zero detection of magnetic field	×	○ [All magnetic tips]
Vector magnetic field measurement	×	○ [Soft magnetic tip]
Stroboscopic measurement of AC magnetic field	×	○ [Hard magnetic tip]
Fixed measuring direction of magnetic field	×	○ [Superparamagnetic tip]
Precise magnetic field measurement on rough surface	×	○ [Superparamagnetic tip]
Simultaneous imaging of DC & AC magnetic field (Spectroscopic measurement of magnetic field)	×	○ [Soft magnetic tip] [Superparamagnetic tip]
Spatial resolution (half of the minimum detectable wavelength)	> 10 nm (Necessary for vacuum atmosphere.)	< 5nm (Air atmosphere is OK.) [Soft magnetic tip] [Hard magnetic tip]
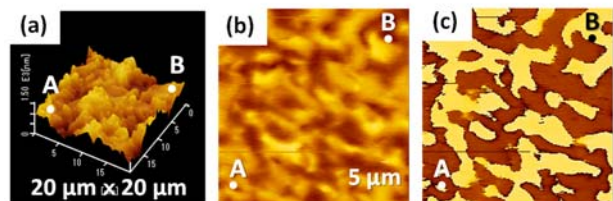
Fig. 1 (a) topographic image, (b) A-MFM signed image of DC magnetic field gradient, (c) A-MFM polarity image of DC magnetic field gradient for a fractured surface of demagnetized anisotropic Sr ferrite sintered magnet.

we have recently developed a sensitive FeCo-Gd$_2$O$_3$ superparamagnetic tip. A-MFM with a superparamagnetic tip enables the precise imaging of near-surface static magnetic field with a fixed direction parallel to the tip magnetic moment driven by AC magnetic field. Even rough fractured surface can be imaged in this way.

Fig, 1 shows A-MFM images on a fractured surface of demagnetized anisotropic Sr ferrite magnet. Fig, 1(a), (b) and (c) are the topographic image, the signed intensity image of DC magnetic field gradient (Lock-in X image) and polarity image of DC magnetic field gradient (Lock-in θ image), respectively. Lock-in amplifier signals of A-MFM as follows.

$$X + iY = R \exp(i\theta) \propto M_z^{ac} \cos(\omega_m t)(\partial^2 H_z^{dc}/\partial z^2) + i\, M_z^{ac} \sin(\omega_m t)(\partial^2 H_z^{dc}/\partial z^2)$$

$$R = \sqrt{X^2 + Y^2} \propto M_z^{ac}(\partial^2 H_z^{dc}/\partial z^2) \propto (\partial^2 H_z^{dc}/\partial z^2)$$

$$H_z^{dc} \Rightarrow -H_z^{dc}, \quad X = M_z^{ac}(\partial^2(-H_z^{dc})/\partial z^2)\cos(\omega_m t) = M_z^{ac}(\partial^2 H_z^{dc}/\partial z^2)\cos(\omega_m t \pm \pi))$$

Here X, R and θ signals correspond to in-phase signed magnetic field gradient, intensity of unsigned magnetic field gradient (absolute value of magnetic field) and phase of magnetic field gradient (The θ change of π corresponds to the polarity change of magnetic field gradient and surface magnetic charge), respectively.

A-MFM can clearly observe DC magnetic field gradient and polarity change of surface magnetic charges in Fig.1 (b) and (c) even on the fractured surface of which surface roughness is about 1μm. On the other hand, the interpretation of conventional MFM image is not easy due to the topography artifact.

The superparamagnetic tip can also solve the problem of ferromagnetic tip that the strong magnetic force of the ferromagnetic tip in high magnetic field from the sample deteriorates the control of constant tip-sample distance near the sample surface. However, the moderate magnetization of superparamagnetic tip prevents its magnetic snapping to the sample surface.

Simultaneous imaging of DC and AC magnetic field by A-MFM is also valid to understand the magnetic homogeneity of magnets by changing the amplitude of AC magnetic field to sample space including a tip and a sample. The magnetic imaging of AC magnetic susceptibility at magnetically reversal area becomes possible.

Fig, 2 shows A-MFM unsigned intensity images of DC and AC magnetic field gradients (Lock-in R images of ω_m and $2\omega_m$ (ω_m : AC magnetic field frequency) under external AC magnetic field with the amplitude of 0.2 and 1.0 kOe for the fracture surface of demagnetized anisotropic Sr ferrite sintered magnet. By using the lock-in R signal of $2\omega_m$ ($\propto M_z^{ac}(\partial^2 H_z^{ac}/\partial z^2)$), the grains having reversible magnetization and generating AC magnetic field can be imaged. With the increase of external AC magnetic field amplitude from 0.2 kOe to 1.0 kOe, the number of magnetically reversible grain increases. These grains have a large scale distribution of DC magnetic field intensities, which source is unvaried magnetization in external AC magnetic field. Simultaneous imaging of DC and AC magnetic field is thought to be useful for analyzing the magnetic inhomogeneity analysis.

In conclusion, our developed A-MFM with the superparamagnetic tip can provide precise magnetic field imaging with a fixed magnetic direction. It is thought to be quite effective method to analyze local magnetic domain structure of various permanent magnets.
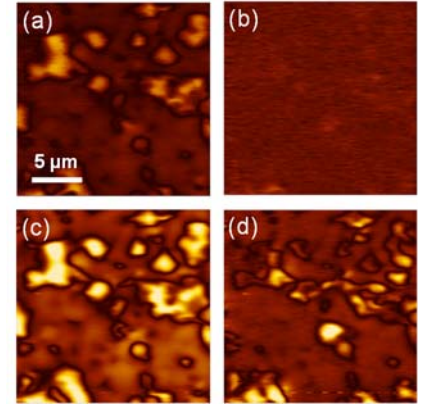
Fig. 2 A-MFM unsigned intensity images of DC magnetic field gradient and AC magnetic field gradient under external AC magnetic field amplitude of 0.2 kOe [(a), (b)] and 1.0 kOe [(c), (d)] for a fractured surface of demagnetized anisotropic Sr ferrite sintered magnet.

References
1) T. Nakamura, A. Yasui, Y. Kotani, T. Fukagawa, T. Nishiuchi, H. Iwai, T. Akiya, T. Ohkubo, Y. Gohda, K. Hono, and S. Hirosawa, Appl. Phys. Lett., 105 (2014) 202404.
2) H. Saito, R. Ito, G. Genta, Z. Li, and S. Yoshimura, J. Appl. Phys., 109 (2011) 07E330.
3) Z. Li, X. Li, D. Liu, H. Saito, and S. Ishio, Nanoscale, 6 (2014) 11163-111168.

More accurate hysteresis curve measurement in large Nd-Fe-B sintered magnets at elevated temperatures

H. Nishio[1], X. H. Yu[2], M. Namba[2], and K. Machida[2]

[1] Research Institute for Measurement of Magnetic Materials, Yokohama 240-0026, Japan

[2] Div. of Applied Chemistry, Osaka University, Suita 565-0871, Japan

The hysteresis curve for large Nd-Fe-B sintered magnets has usually been obtained through the hysteresis graph (HG) method. Recently, widespread discussion has addressed the accuracy limit of hysteresis curve measurement for large Nd-Fe-B sintered magnets at elevated temperatures. The abnormality of magnetization (J) on the hysteresis curve is known to directly affect squareness measurements, such as the differential susceptibility (dJ/dH) near H_{cJ} and H_k/H_{cJ}, in the HG method for Nd-Fe-B sintered magnets with higher coercivity (H_{cJ}) at room temperature, where H and H_k are the magnetic and knee fields, respectively. The abnormality of J is caused by the distortion of magnetic flux distribution around the sample at high fields. To obtain a more accurate hysteresis curve for large Nd-Fe-B sintered magnets at elevated temperatures, we employed a superconducting magnet-based vibrating sample magnetometer (SCM-VSM) with a maximum magnetic field (H_m) of 8 MA/m. The values of dJ/dH near H_{cJ} and H_k/H_{cJ} obtained from the SCM-VSM were compared with those obtained from the HG method at 298 to 473 K. The HG method employed a large electromagnet (H_m of 2.7 MA/m) with improved fixture of heated Fe-Co pole tips. The values of H_{cJ} for the Nd-Fe-B sintered magnet samples A and B were 1.2 and 2.7 MA/m, respectively. The compositions of samples A and B were $Nd_{10.4}Pr_{3.0}Dy_{0.4}Fe_{bal.}Co_{0.6}Al_{0.6}B_{6.1}$ and $Nd_{9.5}Dy_{4.1}Fe_{bal.}Co_{0.6}Al_{0.5}B_{5.8}$, respectively. Cylindrical and spherical samples were machined from the same sintered block for the HG and SCM-VSM measurements, respectively. The cylindrical samples used for the HG method had a diameter (D) of 10 mm and lengths (L) of 7, 14, and 21 mm. A spherical sample with a D of 7 mm was prepared using the two-pipe method for the SCM-VSM measurement. To remove the deteriorated surface layer of approximately 8 μm, all processed samples were chemically etched in 3% HNO_3 solution for 1 min.

In the results obtained from the SCM-VSM and HG (in all cases of L/D) measurements, the values of dJ/dH near H_{cJ} increased gradually as the temperature rose for sample A, which had a lower H_{cJ}. The differences between the values obtained from these methods were small. In contrast, the values of dJ/dH near H_{cJ} obtained from the HG method (in all cases of L/D) increased rapidly as the temperature rose for sample B, which had a higher H_{cJ}, as shown in Fig. 1. The values obtained from the SCM-VSM method gradually decreased as the temperature rose. However, the measured values from the two different methods generally agreed well at temperatures above 423 K, where H_{cJ} was reduced below 1.2 MA/m. The values of H_k/H_{cJ} obtained from the SCM-VSM method at 473 K were superior to those obtained from the HG method (in all cases of L/D) regardless of H_{cJ} (Fig. 2). Greater L/D led to easier uniform magnetization of cylindrical magnets, causing larger L/D to improve dJ/dH near H_{cJ} and H_k/H_{cJ} measurements with the HG method.
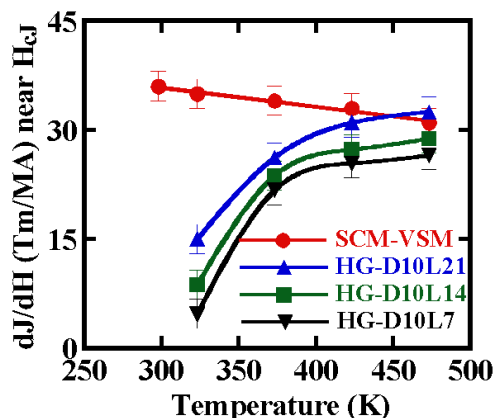

Fig.1 Temperature dependence of dJ/dH near H_{cJ} measured by SCM-VSM and HG methods for Sample B.
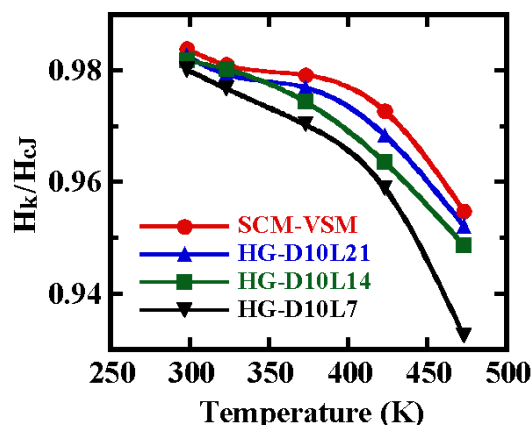
Fig.2 Temperature dependence of H_k/H_{cJ} measured by SCM-VSM and HG methods for Sample A.